Nonlinear vibration response of a helicopter supercritical tail rotor drive shaft equipped with a dry friction damper

Liyao Song, Bai Chen, Bo Li, Rupeng Zhu and Dan Wang
College of Mechanical and Electrical Engineering, Nanjing University of Aeronautics and Astronautics, Nanjing, China

Received 6 September 2022
Revised 26 September 2022
Accepted 26 September 2022

Abstract

Purpose – The supercritical design of tail rotor drive shaft has attracted more attention in helicopter design due to its high power–weight ratio and low maintenance cost. However, there exists excessive vibration when the shaft passes through the critical frequency. Dry friction damper is the equipment applied to the drive shaft to suppress the excessive vibration. In order to figure out the damping mechanism of the dry friction damper and improve the damping efficiency, the dynamic model of the shaft/damper system is established based on the Jeffcott rotor model.

Design/methodology/approach – The typical frequency response of the system is studied through bifurcation diagrams, amplitude-frequency characteristic curves and waterfall frequency response spectrum. The typical transient responses under frequency sweeps are also obtained.

Findings – The results show that the response of the system changes from periodic no-rub motion to quasi-periodic rub-impact motion, and then to synchronous full annular rub-impact, and finally, back to periodic no-rub motion. The slip of the rub-impact ring improves the stability of the system. Besides, the effects of the system parameters including critical dry friction force, rub-impact friction coefficient, initial clearance on the stability and the vibration damping capacity are studied. It is observed that the stability changes significantly varying the three parameters respectively. The vibration damping capacity is mainly affected by the critical dry friction force and the initial clearance.

Originality/value – Presented results provide guidance for the design of the dry friction damper.

Keywords Dry friction damper, Rub-impact, Nonlinear dynamics, Vibration damping

Paper type Research paper

1. Introduction

The tail rotor drive shaft which transmits power from the main reducer to intermediate reducer, then to tail reducer is an important part of the helicopter transmission system (Mei, 2005). It is composed of two parts, including a horizontal tail shaft and an inclined tail shaft as shown in Figure 1. At present, there mainly exist two strategies for helicopter tail rotor drive shaft design: subcritical design (the operating frequency of the drive shaft is below the first natural frequency), supercritical design (the operating frequency of the drive shaft is above the first natural frequency). In subcritical design, many shaft segments and supports are set to ensure the high first critical frequency which results in heavy weight of the transmission

This paper has been funded by the National Natural Science Foundation of China (52005253), the Natural Science Foundation of Jiangsu Province (BK20200426) and the National Key Laboratory of Science and Technology on Helicopter Transmission (HTL-A-21G07, HTL-A-22K01).

Journal of Intelligent Manufacturing and Special Equipment
Vol. 3 No. 2, 2022
pp. 173-191
Emerald Publishing Limited
e-ISSN: 2633-660X
p-ISSN: 2633-6596
DOI 10.1108/JIMSE-09-2022-0014

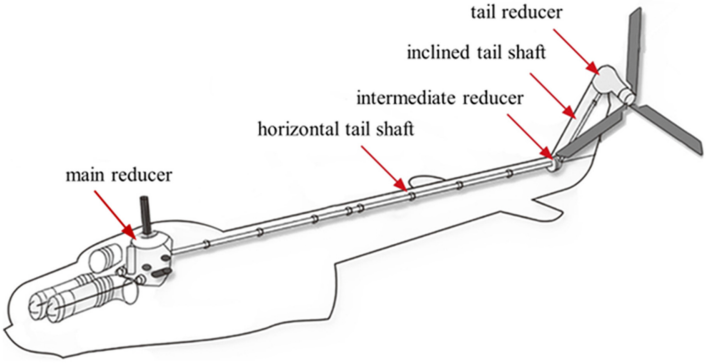

Figure 1.
Model of the helicopter tail drive system

system (Wang, 2012). In supercritical design, considering the lower first critical frequency, fewer supports are set, leading to a reduced weight. The stability of the system is also improved due to fewer segments (Hetherington *et al.*, 1990). With these advantages, the supercritical design of tail rotor drive shaft has attracted more attention in helicopter design. However, in supercritical design, there will be excessive vibration when the shaft passes through the first critical frequency. The excessive vibration can be avoided by using dry friction dampers which are located at the shaft midpoints as shown in Figure 2. Figure 2b shows the section view of a dry friction damper. The damper is mainly composed of a rub-impact ring, two pre-tightening springs, four friction discs, two bolts and a base. There is an initial clearance δ_1 between the drive shaft and the rub-impact ring and an initial clearance δ_2 between the rub-impact ring and the bolt. Specified friction against the side faces of the disc is set by varying the pre-tightening springs force, giving the rub-impact ring resistance force. The rub-impact ring begins to slip when it overcomes the resistance force which is called critical dry friction force in this paper. The excessive vibration of the shaft is restricted by the rub-impact ring, leading to the dynamics of the system being similar to the rub-impact in rotor-stator system. Therefore, the study of rub-impact also has great reference value for the dynamic analysis of the shaft/dry friction damper system.

Rub-impact is a common fault in rotating machinery due to the small clearance between rotor and stator. The dynamics of the system changes considerably due to the rub-impact, especially the occurrence of dry whip (Jiang and Chen, 2013). The dynamic system with rub-impact can be divided into two types: the system with immovable stator and the system with movable stator. Most studies focus on the system with immovable stator which has elastic contact surface. Jeffcott rotor system is one of the most popular disk–shaft rotor models

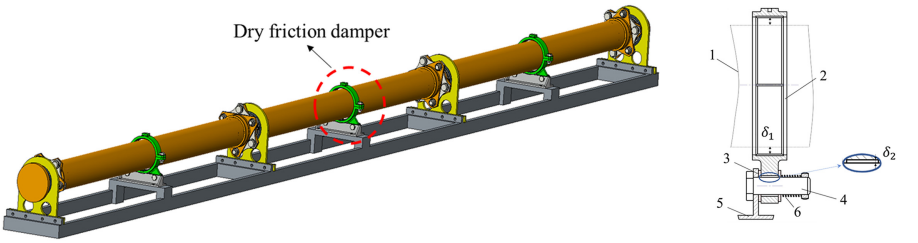

Model of drive shafts with dry friction dampers

(a)

Section view of the dry friction damper

(b)

Figure 2.
Model of the shaft/damper system: 1) shaft, 2) rub-impact ring, 3) friction disc, 4) bolt, 5) base and 6) pre-tightening spring

which are used to study dynamic characteristics of the rotor system with rub-impact (Liu *et al.*, 2015). Jiang *et al.* established the dynamic model of a specific rub-impact system based on the Jeffcott rotor with the stationary stator. The development of the rotor response into dry whip was studied. It was found that the rotor in resonance at a negative (natural) frequency of the system is the physical reason for the onset of dry whip with imbalance. The onset condition of dry whip was also derived by using the method of multiple scales (Jiang and Ulbrich, 2005). After that, he proposed a method to derive the global response characteristics of a piecewise smooth dynamical system with rub-impact. The existence boundaries of no-rub motion, synchronous full annular rub motion, partial rub-impact motion and dry whip were determined, which gave deep insights into the interactive effects of parameters on the dynamic behavior of the model (Jiang, 2009). Hua *et al.* established the dynamic model of a rotor–rubber bearing system with the nonlinear contact stiffness and the Stribeck friction model. The effects of parameters such as rotational speed, the decaying factor in the Stribeck friction model, the linear stiffness coefficient and the nonlinear stiffness coefficient on the dynamic characteristics were studied. It was found that periodic annular rub-impact motion would be more stable with a higher decaying factor and linear stiffness coefficient (Hua *et al.*, 2015). Loïc Peletan *et al.* proposed a quasi-periodic harmonic balance method (HBM) coupled with a pseudo arc-length continuation algorithm to predict the steady-state dynamic behavior of rotor–stator system with rub-impact (Peletan *et al.*, 2014). Ebrahim Tofighi-Niaki *et al.* studied the nonlinear dynamics of a flexible rotor on tilting pad journal bearings with rub–impact (Tofighi-Niaki *et al.*, 2018). Fei *et al.* analyzed the nonlinear vibration behavior of the whole aeroengine including rolling bearing and squeeze film damper under rub-impact fault (Liu *et al.*, 2021). The studies above are focused on the system with a single rotor. K. Prabith *et al.* studied the stability of a two-spool rotor system with rub-impact for two modes of rotor operations including co-rotation and counter-rotation (Prabith and Krishna, 2021). Liu *et al.* studied the dynamic characteristics of a disk–drum–shaft rotor system, in which the coupling of the whole rotor whirl (the motion of the disk) and local drum vibration were both taken into account (Liu *et al.*, 2015). To simulate the rub-impact of the rotor system, Chu *et al.* established an experimental setup with a special structure of stator that could simulate the condition of the full rub. A variety of vibration features of the rub-impact rotor system were observed in the performed experiments under different conditions including one and two rotors with single- and multi-disks (Chu and Lu, 2005). There are relatively few literature studies on the rotor–stator system with movable stators. They can be further divided into two types: with the inertia of the stator (Shang *et al.*, 2010; Bartha, 2000; Jiang *et al.*, 2006); without the inertia of the stators (Dżygadło and Perkowski, 2002). Shang *et al.* established the dynamic model of a rotor–stator system with a movable stator supported by a linear spring. The influence of cross-coupling effects on the dynamics of the systems was investigated (Shang *et al.*, 2010). Besides, there are some special cases in which rub-impact occurs normal (Dai *et al.*, 2001; Sun, 2006; Ishida and Inoue, 2008; Keogh, 2012; Markert, 1998), such as the drive shaft/dry friction damper system in this paper. The studies on dry friction dampers applied to helicopter tail shaft damping are very limited. Özaydın focused on developing the mechanical models of dry friction damper. Based on the macroslip friction model, three mechanical models including one-dimensional model without clearance, one-dimensional model with clearance and two-dimensional model without clearance were developed. The solution of the nonlinear system under the three different mechanical models was obtained respectively by the harmonic balance method and Newton method. The effects of critical dry friction force, initial clearance between shaft and damper and location of the damper on vibration damping capacity were further analyzed (Özaydın, 2017; Özaydin and Cigeroglu, 2017). However, the tangential rub-impact force between shaft and damper which seriously affects the dynamic characteristics of the system was ignored in his study. Dżygadło and Perkowski established a dynamic model of the shaft/damper system with rub-impact, in

which the inertial of the rub-impact ring is neglected. The effects of critical dry friction damper and initial clearance between shaft and damper on resonance amplitude and normal operation of the shaft were mainly analyzed. The results showed that with large critical dry friction force and small clearance, the vibration can be suppressed sufficiently while the response of shaft can be chaotic (Dżygadło and Perkowski, 2000, 2002; Perkowski, 2016). Huang *et al.* established the dynamic model of the system with rub-impact based on the linear contact stiffness and Coulomb friction model. The mechanical model of a damper with dual clearance was developed for the first time. The inertial of the rub-impact ring was also considered. They proposed that increasing the critical dry friction force can improve the damping capacity, but the bifurcation of the system is also more serious. The results show that when the damper sticks, synchronous full annular rub-impact occurs; when the damper slips, local rub-impact occurs (Huang *et al.*, 2021a). They focused on the effects of the occurrence of rub-impact on the dynamic characteristics of the system. The influence of damper parameters other than critical dry friction force was neglected, leading to the design of the damper cannot be further optimized. In their later study, the effects of viscous internal damping of the composite shaft and gyroscopic moment on the phase difference and stability regions of the shaft/damper system were presented (Huang *et al.*, 2021b). However, the damper was regarded as static, resulting in that the shaft/damper system was equal to a typical rotor–stator system with immovable stator actually. From the above research, it can be seen that at present, the study on the dynamic characteristics of shaft/dry friction damper systems is not clear, and the effect of parameters on the dynamic characteristics of the system needs to be further studied.

In this paper, in order to improve the design of the damper, a nonlinear dynamics of a drive shaft/dry friction damper system is analyzed. Studies on typical response of the system and the stability and vibration damping capacity with various parameters are performed. The rest of this paper is organized as follows. In section 2, the dynamic model of the shaft/damper system is established. The mathematical model used to simulate the rub-impact between the shaft and damper and the dry friction force is illustrated. In section 3, numerical results obtained from nonlinear dynamics analysis are presented. The response characteristics of the system are studied by the bifurcation diagrams, amplitude-frequency characteristic curves, and so on. The effects of critical dry friction force, rub-impact friction coefficient, initial clearance on the stability and the vibration damping capacity are studied. Finally, a brief conclusion is made in section 4.

2. Dynamic model of the drive shaft/damper system

2.1 Model description

To analyze this shaft/damper system, the following assumptions are made:

(1) The gyroscopic effects of the shaft are neglected, and only the transverse vibration is taken into account.

(2) The gravity of the shaft and the damper is neglected.

(3) The time during rub-impact is very short; therefore, the impact force can be expressed by an elastic impact model. Also, the frictional relationship is assumed to be Coulomb type.

(4) The rotation of the damper is neglected.

The tail rotor drive shaft is represented by a Jeffcott rotor which consists of a weightless shaft and a rigid disk with mass m_s as shown in Figure 3a. The mass center of the disk is located at a distance e from its geometrical center. The stiffness of the shaft is k_s and the damping coefficient is c_s. The rub-impact ring with mass m_r has an elastic contact surface modeled as a

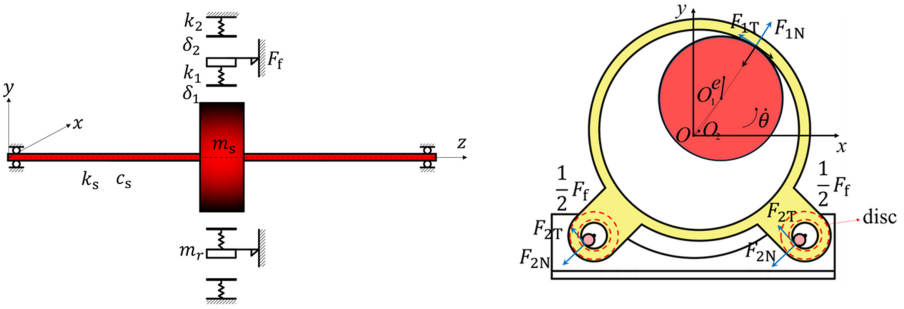

Schematic diagram of the system

(a)

Rub-impact force model

(b)

Figure 3.
Jeffcott rotor system with a dry friction damper

symmetrical set of radial springs with isotropic stiffness k_1, and sliding friction coefficient f_1 in the big hole and stiffness k_2, and sliding friction coefficient f_2 in the two smaller holes. The dry friction force between rub-impact ring and the friction discs is F_f with a pre-tightening force F_s, and the sliding friction coefficient, f_3. The rotor spins with rotational speed $\dot{\theta}$. When the vibration amplitude of the rotor exceeds δ_1, rub-impact occurs between the rotor and the rub-impact ring, called the first rub-impact in this paper. The first radial rub-impact force and tangential rub-impact force are F_{1N} and F_{1T}, respectively. The rub-impact ring begins to move once the rub-impact force exceeds the critical dry friction force. When the radial displacement of the rub-impact exceeds δ_2, rub-impact occurs between the ring and the bolts, called the second rub-impact. The second radial rub-impact force and tangential rub-impact force are F_{2N} and F_{2T}, respectively. The rub-impact forces are shown in Figure 3b. An inertial coordinate system Oxy is set up. O_1 is the geometrical center of the rotor, and O_2 is the geometrical center of the rub-impact ring.

The governing equations of the Jeffcott rotor/dry friction damper system can be written as:

$$\begin{aligned}
m_s\ddot{x}_s + k_s x_s + c_s\dot{x}_s &= m_s\dot{\theta}^2 e\cos\theta + m_s\ddot{\theta}e\sin\theta - F_{1N}\cos\varphi_1 - F_{1T}\sin\varphi_1\\
m_s\ddot{y}_s + k_s y_s + c_s\dot{y}_s &= m_s\dot{\theta}^2 e\sin\theta - m_s\ddot{\theta}e\cos\theta - F_{1N}\sin\varphi_1 - F_{1T}\cos\varphi_1\\
m_r\ddot{x}_r &= F_{1N}\cos\varphi_1 - F_{1T}\sin\varphi_1 + 2(F_{2N}\cos\varphi_2 - F_{2T}\sin\varphi_2) - |F_f|\cos\beta\\
m_r\ddot{y}_r &= F_{1N}\sin\varphi_1 + F_{1T}\cos\varphi_1 + 2(F_{2N}\sin\varphi_2 + F_{2T}\cos\varphi_2) - |F_f|\sin\beta
\end{aligned} \tag{1}$$

where x_s, y_s are the instantaneous positions of the rotor along x, y directions, respectively, and x_r, y_r are the instantaneous positions of the rub-impact ring along x, y directions, respectively; φ_1, φ_2 are the angles between radial rub-impact forces and x-axis. β is the angle between the speed direction of the rub-impact ring and x-axis. φ_1, φ_2 and β can be obtained by the following equations.

$$\begin{aligned}
\cos\varphi_1 &= (x_s - x_r)\left((x_s - x_r)^2 + (y_s - y_r)^2\right)^{-1/2}\\
\sin\varphi_1 &= (y_s - y_r)\left((x_s - x_r)^2 + (y_s - y_r)^2\right)^{-1/2}
\end{aligned} \tag{2}$$

$$\begin{aligned}
\cos\varphi_2 &= -x_r\left(x_r^2 + y_r^2\right)^{-1/2}\\
\sin\varphi_2 &= -y_r\left(x_r^2 + y_r^2\right)^{-1/2}
\end{aligned} \tag{3}$$

$$\cos\beta = \dot{x}_r(\dot{x}_r^2 + \dot{y}_r^2)^{-1/2}$$
$$\sin\beta = \dot{y}_r(\dot{x}_r^2 + \dot{y}_r^2)^{-1/2} \tag{4}$$

2.2 Rub-impact force

The first and second radial rub-impact forces can be expressed as

$$F_{1N} = \Theta(\varepsilon_1)k_1\varepsilon_1$$
$$F_{2N} = \Theta(\varepsilon_2)k_2\varepsilon_2 \tag{5}$$

where $\Theta(\varepsilon_1), \Theta(\varepsilon_2)$ are the Heaviside functions which can be expressed as

$$\Theta(\varepsilon) = \begin{cases} 0, & \varepsilon \le 0 \\ 1, & \varepsilon > 0 \end{cases} \tag{6}$$

ε_1 is the contact depth between the rotor and the rub-impact ring at the contact point. It can be expressed as:

$$\varepsilon_1 = \left((x_s - x_r)^2 + (y_s - y_r)^2\right)^{1/2} - \delta_1 \tag{7}$$

ε_2 is the contact depth between the rub-impact ring and the bolts at the contact point. It can be expressed as:

$$\varepsilon_2 = (x_r^2 + y_r^2)^{1/2} - \delta_2 \tag{8}$$

The tangential rub forces can be represented as:

$$F_{1T} = \Theta(\varepsilon_1)f_1F_{1N}\text{sign}(v_1)$$
$$F_{2T} = \Theta(\varepsilon_2)f_2F_{2N}\text{sign}(v_2) \tag{9}$$

where v_1 is the tangential relative velocity between the rotor and rub-impact ring at the contact point. It can be calculated as follows.

$$v_1 = (\dot{y}_s - \dot{y}_r)\cos\varphi_1 - (\dot{x}_s - \dot{x}_r)\sin\varphi_1 + \dot{\theta}\frac{D}{2} \tag{10}$$

where D is the diameter of the drive shaft. v_2 is the tangential relative velocity between the rub-impact ring and the bolts at the contact point. It can be calculated as follows.

$$v_2 = -\dot{y}_r\cos\varphi_2 + \dot{x}_r\sin\varphi_2 \tag{11}$$

2.3 Dry friction force

The dry friction force between the rub-impact ring and the friction discs can be expressed as (Pennestri *et al.*, 2016):

$$F_f = f_3F_s\tanh\left(\frac{(\dot{x}_r^2 + \dot{y}_r^2)^{1/2}}{v_d}\right) \tag{12}$$

where v_d is the velocity tolerance. f_3F_s is the critical dry friction force expressed as F_{pre} in this paper.

For the convenience of the computation and discussion, the dimensionless transformations of some parameters and results in this research are given as follows.

$$M_s = \frac{m_s}{m_s} = 1, K_s = \frac{k_s}{k_s} = 1, \xi_s = \frac{c_s}{2}(k_s m_s)^{-1/2}, \Omega = \frac{\dot{\theta}}{\omega_n}, M_r = \frac{m_r}{m_s},$$
$$K_1 = \frac{k_1}{k_s}, \Delta_1 = \frac{\delta_1}{e}, K_2 = \frac{k_2}{k_s}, \Delta_2 = \frac{\delta_2}{e}, F_p = \frac{F_{pre}}{k_s e} \quad (13)$$

where ω_n is the natural frequency of the drive shaft expressed as $\omega_n = (\frac{k_s}{m_s})^{1/2}$.

3. Analysis of typical response regimes

The typical response of the system is obtained in this section. Firstly, the typical frequency response regimes are illustrated by the bifurcation diagram, amplitude-frequency characteristic curves and the waterfall frequency response spectrum. After that, the transient responses to the frequency sweeps through resonance are studied. Parameter values of an example helicopter tail drive shaft are given in Table 1 and the dimensionless parameter values of the dry friction damper are given in Table 2.

3.1 Typical frequency response regimes

Considering the rotational speed of the rotor as the control parameter, the frequency responses are obtained in this section. Reaching the steady-state condition is guaranteed by running 150 cycles and taking the last 50 cycles. Figure 4a shows the bifurcation diagrams

Table 1. Parameters of an example helicopter tail drive shaft

Parameter	m_s/kg	k_s/(kN/m)	c_s/(Ns/m)	e/(mm)
Value	2	180	24	0.3

Table 2. Dimensionless parameters of dry friction damper

Parameter	M_r	K_1	f_2	K_2	f_3	Δ_1	Δ_2	F_p
Value	0.05	15	0.02	25	0.02	3	5	2

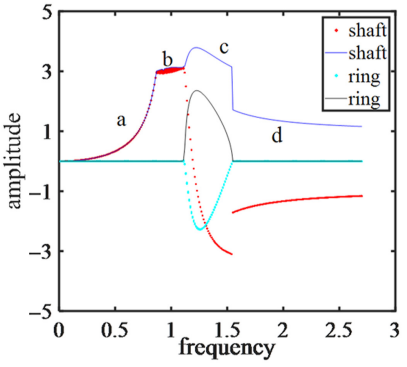

Bifurcation diagrams and amplitude frequency characteristic curves

(a)

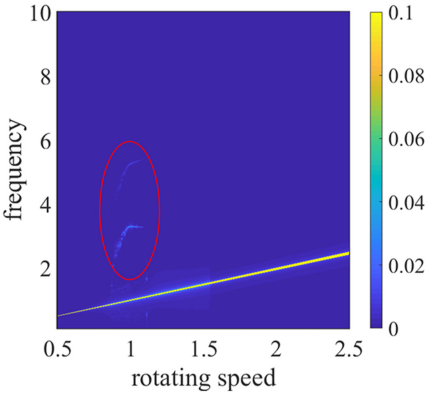

Waterfall frequency response spectrum

(b)

Figure 4. Typical upward frequency response

and amplitude frequency characteristic curves of the rotor and the rub-impact ring during upward frequency. The red dot and blue (or purple?) curve represent the bifurcation diagram and the amplitude–frequency characteristic curve of the rotor, respectively. The cyan dot and black curve represent the bifurcation diagram and the amplitude–frequency characteristic curve of the rub-impact ring respectively. The waterfall frequency response spectrum in Figure 4b gives a summary of frequency content of the behavior of the rotor during upward frequency.

From Figure 4a, the movement of the drive shaft can be divided into four stages: stage a at the interval of $\Omega < 0.87$, stage b at the interval of $0.87 < \Omega < 1.11$, stage c at the interval of $1.11 < \Omega < 1.54$ and stage d at the interval of $\Omega > 1.54$. At stage a, the vibration amplitude of the rotor is smaller than Δ_1 and the rub-impact phenomenon between the rotor and the rub-impact ring does not occur.

Figure 5 shows the typical pictures of whirling orbit, phase trajectory, Poincaré map and frequency spectrum of the rotor with $\Omega = 0.6$. In the whirling orbits, the red circle indicates the initial clearance. It can be seen that the response of the rotor is periodic no-rub motion in this interval. At stage b, the vibration amplitude exceeds Δ_1, which means the occurrence of the rub-impact. But the ring remains stationary because of the friction force.

Figure 6 shows the whirling orbit, phase trajectory, Poincaré map and frequency spectrum of rotor with $\Omega = 1$, respectively. It can be seen that the response is full annular rub-impact. The bifurcation is a circle, which means that the motion of the rotor is quasi-periodic. In addition to the excitation frequency, there are high-order harmonics caused by the rub-impact

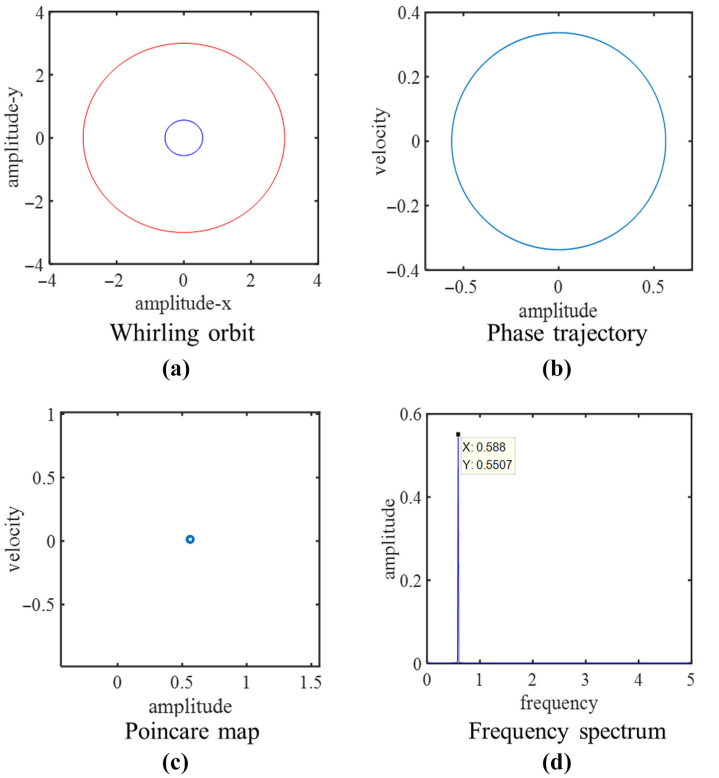

Figure 5.
Periodic no-rub motion at $\Omega = 0.6$

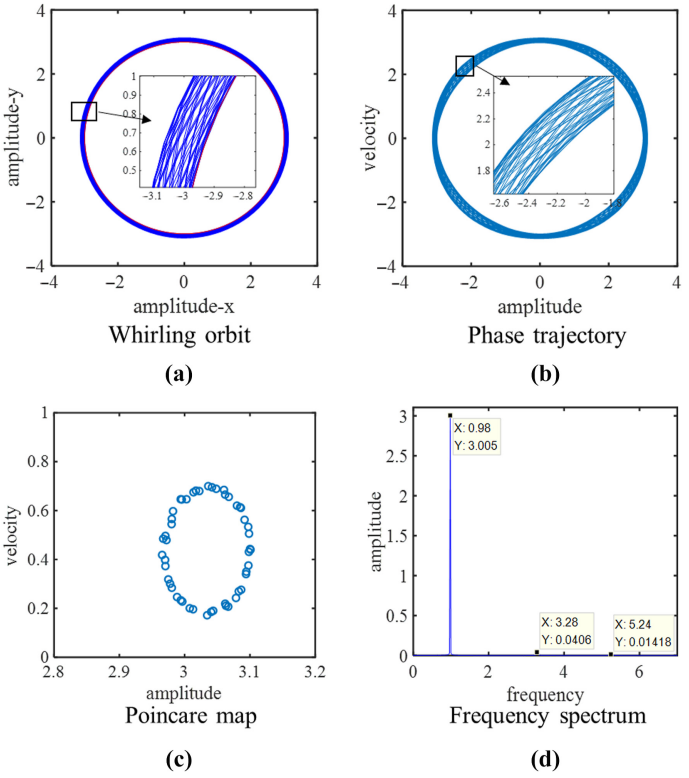

Figure 6.
Quasi-periodic annular rub-impact motion at $\Omega = 1$

in frequency spectrum. The ratios of the high-order harmonics to the excitation frequency are about 3.3 and 5.3. In this interval, the response becomes unstable. With the excitation frequency increasing and approaching the critical speed of the rotor system, the rub-impact force increases. At stage c, the rub-impact force overcomes the critical dry friction force and the rub-impact ring begins to move.

Figure 7 shows the whirling orbit, phase trajectory, Poincaré map and frequency spectrum of the rotor with $\Omega = 1.2$. It can be seen that the rotor keeps contact with the rub-impact ring and rotates synchronously. The responses of the rotor and the rub-impact ring are both period-one motion. Synchronous full annular rub-impact occurs and the system is relatively stable in this interval. At $\Omega = 1.54$, a jump phenomenon occurs and the amplitude of the drive shaft decreases rapidly.

At stage d, the amplitude of the rotor is smaller than Δ_1 and there is no rub-impact again. The response of the rotor is back to period-one motion. Stage d is the operating frequency range of the drive shaft. The jump frequency determines the lower boundary of the normal frequency range. Therefore, the jump frequency is an important factor to be considered in the parameter design of the damper.

It can be concluded that the response of the rotor changes from periodic no-rub motion to quasi-periodic rub-impact motion, and then to synchronous full annular rub-impact, finally, back to periodic no-rub motion. The system is unstable in the interval of quasi-periodic rub-impact motion, but it becomes stable in the interval of synchronous full annular rub-impact motion due to the slip of the rub-impact ring. The rotor maintains forward whirling in the whole frequency range.

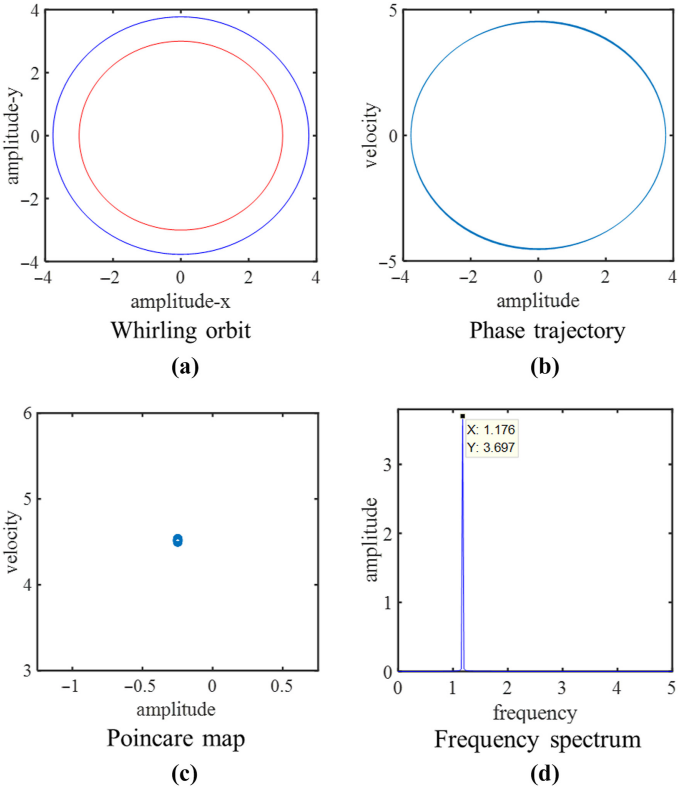

Figure 7.
Periodic no-rub motion at $\Omega = 1.2$

The bifurcation diagrams, amplitude frequency characteristic curves and waterfall frequency response spectrum during downward frequency are depicted in Figure 8a and b respectively. It can be seen that the jump frequency during downward frequency is different

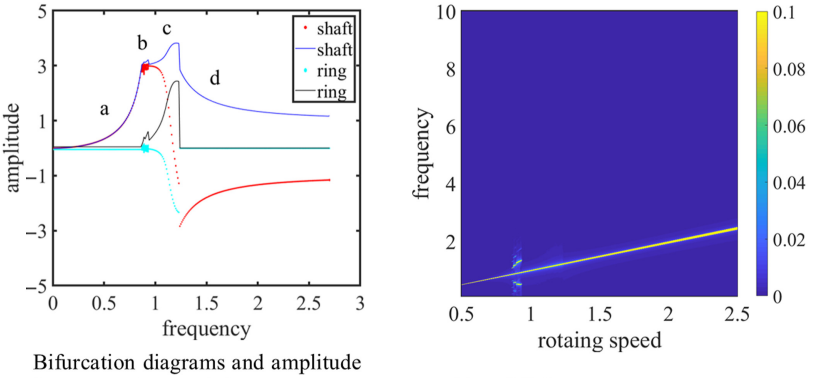

Figure 8.
Typical downward frequency response

from that during upward frequency. In stage b, the rub-impact ring changes from motion to static and the unstability of the system increases. In addition, the dynamic characteristics of the rotor are consistent with each other between the downward and upward frequency.

3.2 Typical transient response under frequency sweeps

The transient response of the rotor is depicted in Figure 9. For a comparison, the response of the rotor without damper is depicted by the gray dotted line. The orange solid line represents the result of upward sweep, and the cyan dotted line represents the result of downward sweep. The amplitude-frequency characteristic curves, determined in frequency response above, are also depicted as shown by the red and blue lines. It can be seen that the transient response of the shaft is consistent with the frequency response. Due to the jump phenomenon, the results of upward sweep and downward sweep are different. The resonance amplitude of the rotor without damper is 24.23, and the resonance amplitude with damper is 3.79. It can be seen that the vibration of the rotor is reduced by 84% with the damper.

3.3 Response with the second rub-impact

In the above typical response, the rub-impact between the rub-impact ring and the base does not occur. Adjusting the second clearance to 2 to makes the second rub-impact occur; the results are shown in Figure 10. The orange solid line represents the response of the rotor only with the first rub-impact, and the cyan dotted line represents the response with the second

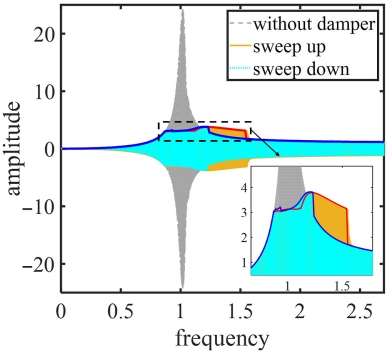

Figure 9.
Transient responses of the rotor

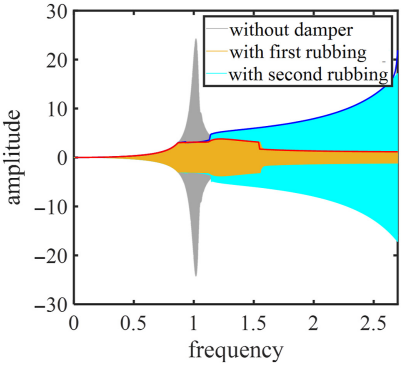

Figure 10.
Responses of the rotor with second rub-impact

rub-impact. It can be seen that the vibration amplitude of the rotor increases greatly when the second rub-impact occurs. Therefore, in the following analysis, the second clearance is set large to avoid the second rub-impact.

4. Effects of the parameters

4.1 Effects of the critical dry friction force

The effect of critical dry friction force on the response is analyzed by varying the value of F_P. Figure 11 shows the rotor frequency responses with different values of F_P. Figure 11a shows the bifurcation diagrams and amplitude-frequency characteristic curves of the rotor when frequency increases. Figure 11b shows the responses when frequency decreases. It can be seen that as F_P increases, the frequency range of quasi-periodic rub-impact motion increases. The waterfall frequency response spectra are depicted in Figure 12 for different values of critical dry friction force. It can be seen that as the value of F_P increases, higher harmonics occurs and amplitude of the higher harmonics increases simultaneously. Figure 13a shows the transient responses of the rotor to upward frequency sweeps through resonance for different values of F_P. Figure 13b shows the transient responses during downward sweep. The variation of amplitude maximum and jump frequency with different values of F_P is depicted in Figure 14. It can be seen that with the increase of critical dry friction force, the amplitude maximum of the shaft first decreases and then increases, and the jump frequency

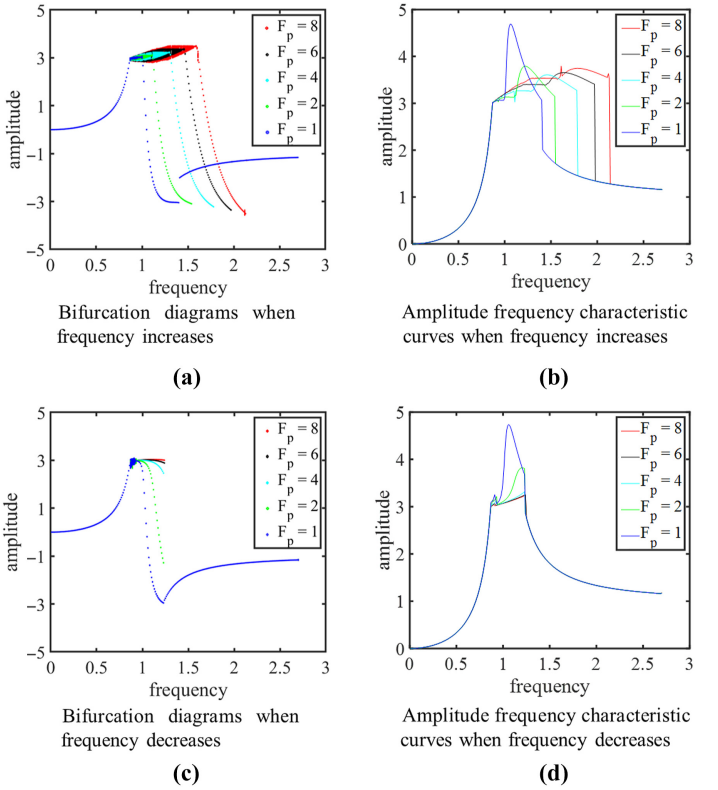

Figure 11.
Bifurcation diagrams and amplitude-frequency characteristic curves for different values of F_P

gradually increases. There is an optimum critical dry friction which minimizes the vibration amplitude of the shaft in the maxima curve.

4.2 Effects of the rub-impact friction coefficient

The effect of rub-impact friction coefficient on the response is analyzed by varying the value of f_1. Figure 15 shows the frequency responses with different values of f_1. The bifurcation diagrams and amplitude-frequency characteristic curves of the drive shaft are depicted in Figure 15a when frequency increases. Figure 15b shows the response when frequency

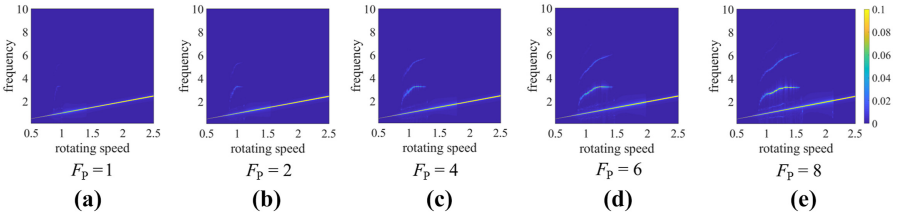

Figure 12.
Waterfall frequency response spectra for different values of F_P during upward frequency

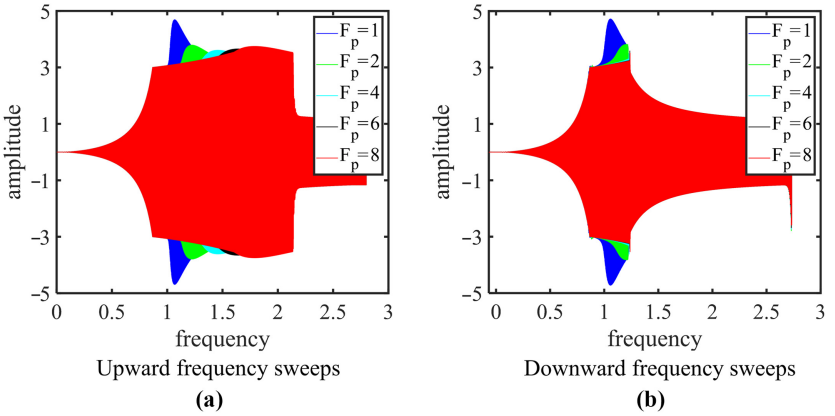

Figure 13.
Transient responses for different values of F_P

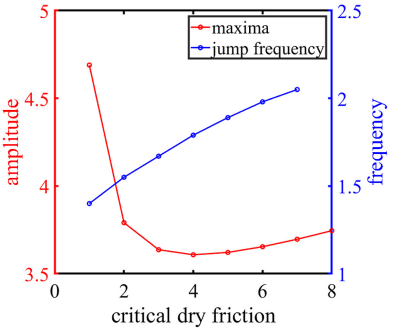

Figure 14.
Variation of maxima amplitude and jump frequency with different values of F_P during upward sweep

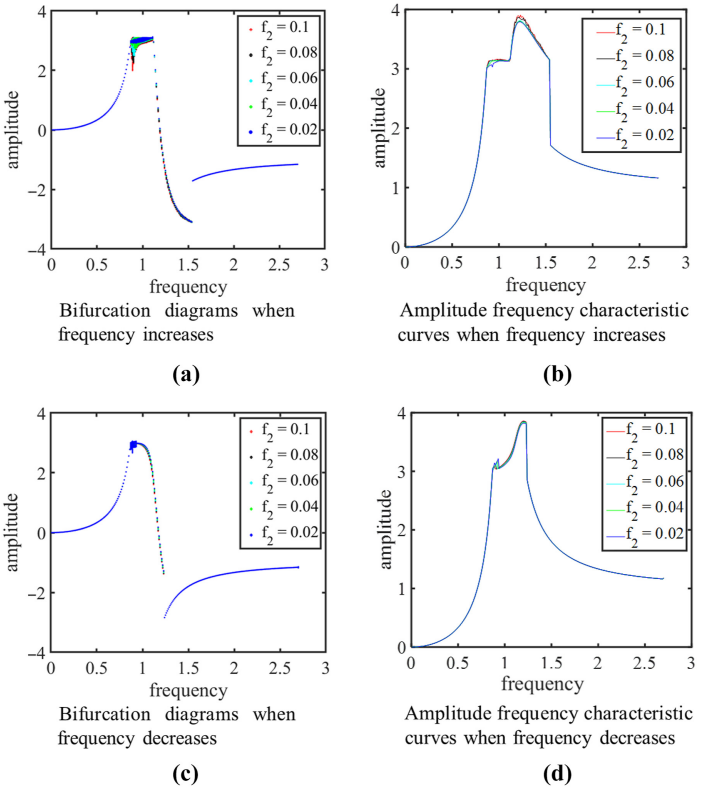

Figure 15.
Bifurcation diagrams and amplitude frequency characteristic curves for different values of f_1

decreases. It is observed that the rub-impact friction coefficient mainly has effect on quasi-periodic rub-impact motion in stage b while no effect on the other stages. The quasi-periodic rub-impact becomes severe and the system becomes unstable as friction coefficient increases. The waterfall frequency response spectra are depicted in Figure 16 for different values of f_1. It is observed that the system oscillates mainly by the primary harmonic, but the amplitude of higher harmonics gradually increases with the increase of f_1. The resonance amplitude and jump frequency are both not affected. Figure 17a shows the transient responses of the rotor to upward frequency sweeps through resonance for different values of f_1. Figure 17b shows the transient responses during downward sweep. The variation of amplitude maximum and jump frequency with different values of f_1 is depicted in Figure 18. It also shows that the

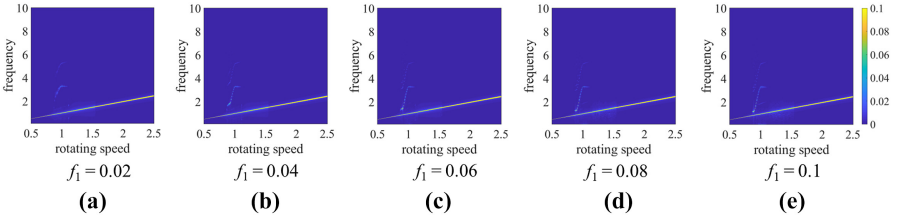

Figure 16.
Waterfall frequency response spectra for different values of f_1 during upward frequency

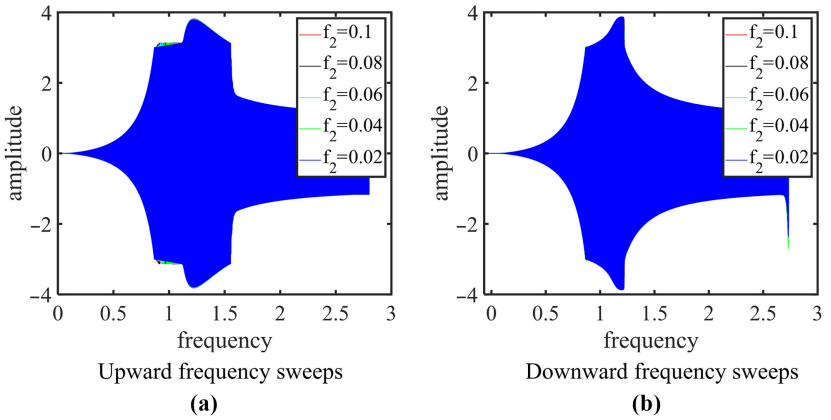

Figure 17.
Transient responses for different values of f_1

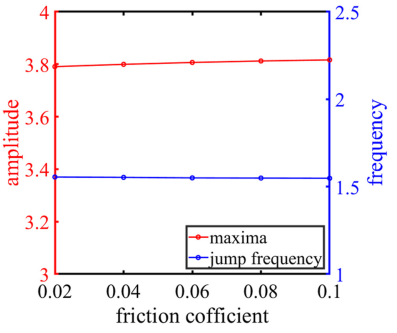

Figure 18.
Variation of maxima amplitude and jump frequency with different values of f_1 during upward sweep

resonance amplitude and jump frequency are almost not affected by the friction coefficient. It can be concluded that the rub and impact between the shaft and the ring becomes lighter as the rub-impact friction coefficient decreases.

4.3 Effects of the initial clearance

The effect of initial clearance on the response is analyzed by varying the value of Δ_1. Figure 19 shows the rotor frequency response with different values of Δ_1. Figure 19a shows the bifurcation diagrams and amplitude-frequency characteristic curves of the rotor when frequency increases. Figure 19b shows the responses when frequency decreases. It can be seen that as Δ_1 decreases, the frequency range of quasi-periodic rub-impact motion increases, and the rub-impact between the shaft and the rub-impact ring become severe. The waterfall frequency response spectra are depicted in Figure 20 for different values of Δ_1. It demonstrates that the system oscillates mainly by the primary harmonic; but higher harmonics occurs with the decrease of Δ_1. The transient responses of the rotor during upward sweep and downward sweep with different values of Δ_1 are plotted in Figure 21. The variation of the maximum amplitude and jump frequency with different values of Δ_1 during upward sweep is depicted in Figure 22. The dotted line indicates that there is no jump before the rotor accelerates to the operating frequency due to the small clearance. It is observed that as Δ_1 decreases, the resonance amplitude decreases while the jump frequency increases. It

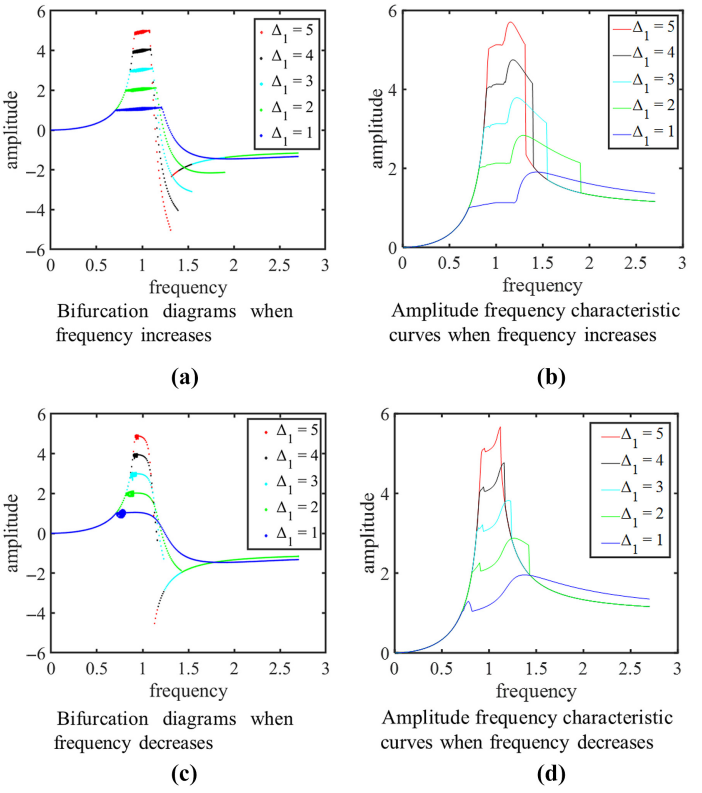

Figure 19.
Bifurcation diagrams and amplitude-frequency characteristic curves for different values of Δ_1

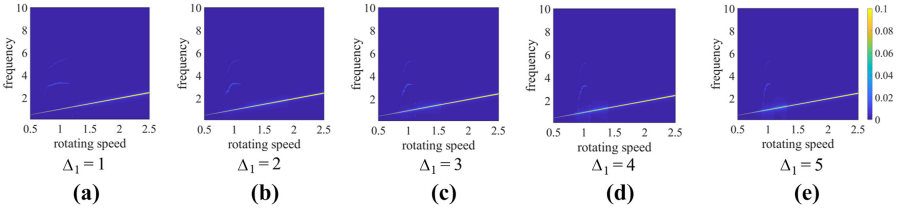

Figure 20.
Waterfall frequency response spectra for different values of Δ_1 during upward frequency

can be concluded that the damper with a small initial clearance can effectively suppress the vibration amplitude. But too small clearance will make the rub-impact between the shaft and the rub-impact ring severe, and this will causes the abnormal operation of the drive shaft eventually.

5. Discussion and conclusions

In this article, a mathematical model has been established to investigate the dynamic characteristics of the supercritical tail rotor drive shaft and the dry friction damper system. The effects on the stability and the vibration damping capacity of critical dry friction force, rub-impact friction coefficient and initial clearance are analyzed in detail. The typical conclusions are summarized as follows.

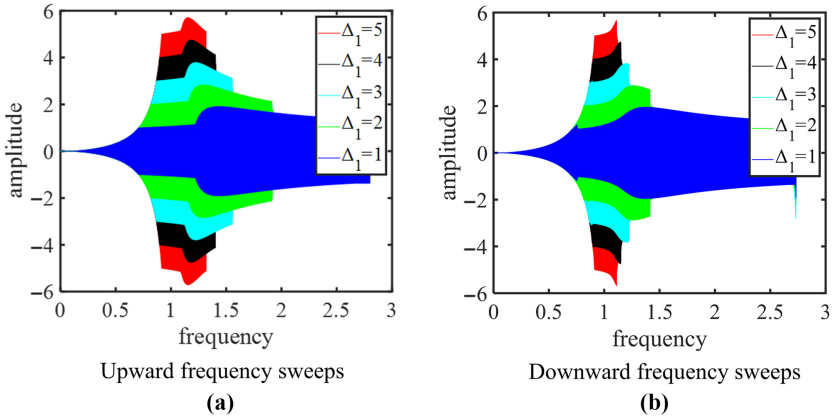

Figure 21.
Transient responses for different values of Δ_1

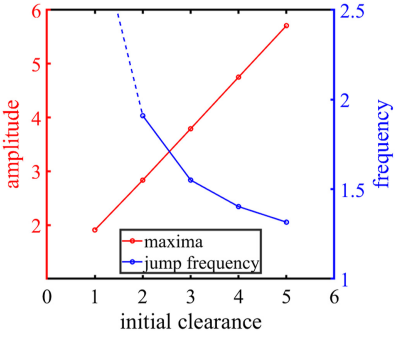

Figure 22.
Variation of maxima amplitude and jump frequency with different values of Δ_1 during upward sweep

The typical frequency response of the shaft/damper system is analyzed by bifurcation diagrams, diagrams of amplitude-frequency characteristic curves and waterfall frequency response spectrum. With the increase of frequency, the response of rotor is divided into four stages, including periodic no-rub motion, quasi-periodic rub-impact motion, synchronous full annular rub-impact motion and periodic no-rub motion. There are higher harmonics in the interval of quasi-periodic rub-impact motion. The whirling orbits, phase trajectories, Poincaré maps and frequency spectrum are derived to study the characteristics of the system in each stage. It is found that the system is unstable in the interval of quasi-periodic rub-impact motion, but it becomes stable in the interval of synchronous full annular rub-impact motion due to the slip of the rub-impact ring.

Finally, a parametric analysis is conducted to investigate the effect of different parameters on the stability and vibration damping capacity. The parameters including critical dry friction, rub-impact friction coefficient and initial clearance are varied individually by keeping the others constant. It is observed that with the increase of critical dry friction, the stability of the system decreases, the resonance amplitude decreases firstly and then increases, and the jump frequency increases. As the rub-impact friction coefficient increases, the system becomes unstable while the vibration amplitude and jump frequency are mostly not affected. With the decrease of the initial clearance between the shaft and the rub-impact ring, the stability and the resonance amplitude both decrease but the jump frequency increases.

According to the parametric analysis, the optimum value of critical dry friction force should be defined at the point with the minimum resonance amplitude in the maxima curve or the left of this point. The rub-impact surface between the rotor and the rub-impact ring should be designed as smooth as possible. A small initial clearance between the drive shaft and the rub-impact ring can suppress the vibration sufficiently but affects the normal working of the drive shaft. Therefore, the initial clearance should not be designed too small.

References

Bartha, A.R. (2000), "Dry friction backward whirl of rotors", PhD Thesis, ETH Zurich, Zurich.

Chu, F. and Lu, W. (2005), "Experimental observation of nonlinear vibrations in a rub-impact rotor system", *Journal of Sound and Vibration*, Vol. 283 Nos 3-5, pp. 621-643.

Dai, X., Zhang, X. and Jin, X. (2001), "The partial and full rubbing of a flywheel rotor–bearing–stop system", *International Journal of Mechanical Sciences*, Vol. 43 No. 2, pp. 505-519.

Dżygadło, Z. and Perkowski, W. (2000), "Nonlinear dynamic model for flexural vibrations analysis of a supercritical helicopter's tail rotor drive shaft", *Prace-instytut lotnictwa*, Vol. 160, pp. 49-53.

Dżygadło, Z. and Perkowski, W. (2002), "Research on dynamics of a supercritical propulsion shaft equipped with a dry friction damper", *Aircraft Engineering and Aerospace Technology*, Vol. 74 No. 5, pp. 447-454.

Hetherington, P.L., Kraus, R.F. and Darlow, M.S. (1990), "Demonstration of a supercritical composite helicopter power transmission shaft", *Journal of the American Helicopter Society*, Vol. 35 No. 1, pp. 23-28.

Hua, C., Rao, Z., Ta, N. and Zhu, Z. (2015), "Nonlinear dynamics of rub-impact on a rotor-rubber bearing system with the Stribeck friction model", *Journal of Mechanical Science and Technology*, Vol. 29 No. 8, pp. 3109-3119.

Huang, Z., Tan, J., Liu, C. and Lu, X. (2021a), "Dynamic characteristics of a segmented supercritical driveline with flexible couplings and Dry Friction Dampers", *Symmetry*, Vol. 13 No. 2, p. 281.

Huang, Z., Tan, J. and Lu, X. (2021b), "Phase difference and stability of a shaft mounted a dry friction damper: effects of viscous internal damping and gyroscopic moment", *Advances in Mechanical Engineering*, Vol. 13 No. 3, 1687814021996919.

Ishida, Y. and Inoue, T. (2008), "Vibration characteristics of a rotor system in contact with a backup bearing: cases with various failure patterns of the active magnetic bearing", *Journal of Vibration and Control*, Vol. 14 No. 4, pp. 571-589.

Jiang, J. (2009), "Determination of the global responses characteristics of a piecewise smooth dynamical system with contact", *Nonlinear Dynamics*, Vol. 57 No. 3, pp. 351-361.

Jiang, J. and Chen, Y. (2013), "Advances in the research on nonlinear phenomona in rotor/stator rubbing systems", *Advances in Mechanics*, Vol. 43 No. 1, pp. 132-148.

Jiang, J. and Ulbrich, H. (2005), "The physical reason and the analytical condition for the onset of dry whip in rotor-to-stator contact systems", *Journal of Vibration and Acoustics*, Vol. 127 No. 6, pp. 594-603.

Jiang, J., Ulbrich, H. and Chavez, A. (2006), "Improvement of rotor performance under rubbing conditions through active auxiliary bearings", *International Journal of Non-linear Mechanics*, Vol. 41 No. 8, pp. 949-957.

Keogh, P.S. (2012), "Contact dynamic phenomena in rotating machines: active/passive considerations", *Mechanical Systems and Signal Processing*, Vol. 29, pp. 19-33.

Liu, L., Cao, D. and Sun, S. (2015), "Dynamic characteristics of a disk–drum–shaft rotor system with rub-impact", *Nonlinear Dynamics*, Vol. 80 No. 1, pp. 1017-1038.

Liu, J., Fei, Q., Wu, S. and Zhang, D. (2021), "Nonlinear vibration response of a complex aeroengine under the rubbing fault", *Nonlinear Dynamics*, Vol. 106 No. 3, pp. 1869-1890.

Markert, R. (1998), "Transient vibration of elastic rotors in retainer bearings", *Proc. ISROMAC-7*, pp. 764-774.

Mei, Q. (2005), "Dynamics design of helicopter drive shafts", *Journal of Mechanical Transmission*, Vol. 29 No. 5, pp. 19-22.

Özaydın, O. (2017), "Vibration reduction of helicopter tail shaft by using dry friction dampers", Master Thesis, Middle East Technical University, Ankara.

Özaydin, O. and Cigeroglu, E. (2017), "Effect of dry friction damping on the dynamic response of helicopter tail shaft", in Di Maio, D. and Castellini, P. (Eds), *Rotating Machinery, Hybrid Test Methods, Vibro-Acoustics and Laser Vibrometry, Volume 8. Conference Proceedings of the Society for Experimental Mechanics Series*. Springer, Cham. pp. 23-30.

Peletan, L., Baguet, S., Torkhani, M. and Jacquet-Richardet, G. (2014), "Quasi-periodic harmonic balance method for rubbing self-induced vibrations in rotor–stator dynamics", *Nonlinear Dynamics*, Vol. 78 No. 4, pp. 2501-2515.

Pennestri, E., Rossi, V., Salvnial, P. and Valentini, P.P. (2016), "Review and comparison of dry friction force models", *Nonlinear Dynamics*, Vol. 83 No. 4, pp. 1785-1801.

Perkowski, W. (2016), "Dry friction damper for supercritical drive shaft", *Journal of KONES*, Vol. 23 No. 4, pp. 389-396.

Prabith, K. and Krishna, I.R.P. (2021), "The stability analysis of a two-spool rotor system undergoing rub-impact", *Nonlinear Dynamics*, Vol. 104 No. 2, pp. 941-969.

Shang, Z., Jiang, J. and Hong, L. (2010), "The Influence of the cross-coupling effects on the dynamics of rotor/stator rubbing", in Luo, A. (Eds), *Dynamical Systems*. Springer, New York, NY, pp. 121-132.

Sun, G. (2006), "Rotor drop and following thermal growth simulations using detailed auxiliary bearing and damper models", *Journal of Sound and Vibration*, Vol. 289 Nos 1-2, pp. 334-359.

Tofighi-Niaki, E., Asgharifard-Sharabiani, P. and Ahmadian, H. (2018), "Nonlinear dynamics of a flexible rotor on tilting pad journal bearings experiencing rub–impact", *Nonlinear Dynamics*, Vol. 94 No. 4, pp. 2937-2956.

Wang, X. (2012), "Research on the effects of viscoelastic damper to the dynamics of helicopter drive shaft system", Master Thesis, Nanjing University of Aeronautics and Astronautics, Nanjing.

Corresponding author
Dan Wang can be contacted at: wangdan_053@nuaa.edu.cn